ISSN 1063-7826, Semiconductors, 2018, Vol. 52, No. 5, pp. 565–571. © Pleiades Publishing, Ltd., 2018.

XXV INTERNATIONAL SYMPOSIUM
"NANOSTRUCTURES: PHYSICS AND TECHNOLOGY",
SAINT PETERSBURG, RUSSIA, JUNE 26–30, 2017.
EXCITONS IN NANOSTRUCTURES

The Impact of the Substrate Material on the Optical Properties of 2D WSe_2 Monolayers[1]

L. M. Schneider[a2], S. Lippert[a2], J. Kuhnert[a2], D. Renaud[a], K. N. Kang[b], O. Ajayi[c], M.-U. Halbich[a], O. M. Abdulmunem[a], X. Lin[a], K. Hassoon[a], S. Edalati-Boostan[a], Y. D. Kim[c], W. Heimbrodt[a], E. H. Yang[b], J. C. Hone[c], and A. Rahimi-Iman[a]*

[a] *Department of Physics and Materials Sciences Center, Philipps-Universität, Marburg, 35032 Germany*
[b] *Department of Mechanical Engineering, Stevens Institute of Technology, Hoboken, New Jersey, 07030 USA*
[c] *Department of Mechanical Engineering, Columbia University, New York, 10027 USA*
**e-mail: a.r-i@physik.uni-marburg.de*

Received December 25, 2017

Abstract—2D-materials, especially transition metal dichalcogenides (TMDs) have drawn a lot of attention due to their remarkable characteristics rendering them a promising candidate for optical applications. While the basic properties are understood up to now, the influence of the environment has not been studied in detail, yet. Here we highlight a systematic comparison of the optical properties of tungsten diselenide monolayers on different substrates. Subtle changes in the emission spectrum and Raman signature have been found as well as surprisingly pronounced differences in the pump-power-dependent and time-resolved output at higher excitation densities. For all samples, exciton–exciton annihilation can be obtained. Nevertheless an analysis of different pump-dependent decay rates suggests substrate-dependent changes in the diffusion constant as well as exciton Bohr radius.

DOI: 10.1134/S1063782618050275

1. INTRODUCTION

Transition metal dichalcogenide (TMD) monolayers (MLs) have been proposed as a promising candidate for future electro-optical applications due their extraordinary strong interaction with the light field [1–3] and a semiconductorlike band structure—unlike graphene. This enables the design of photodetectors and transistors consisting only of a few atomic layers [4–7]. Indeed, 2D semiconducting materials act as nearly perfect quantum wells with strong confinement potential for charge carriers of the sheet materials, whose wave function is mainly given by the d-orbitals of the transition metal layer [8]. Particularly, the formation and dynamics of excitons are of interest in this field, which, due to their small height, may penetrate surrounding materials below and on top of the material [9]. In this context of exciton studies, elevated fluences gave rise to the observation of biexcitons [10–12], exciton–exciton annihilation [13–17], and the Mott-transition [2, 18].

Yet, to understand the behavior of excitons in these materials better, a systematic study of the influence of the environment—in particular the substrate—is crucial. Recently, there have been studies observing a change in exciton binding energy, exciton radius and doping level at changing dielectric environment [9, 15, 19–22]. Nevertheless, the impact on excitons and the optical properties of TMDs is not yet completely understood and a comparative study involving microphotoluminescence (PL), Raman signal and PL-decay dynamics is missing. Here, we present one such study for tungsten diselenide (WSe_2) MLs on three different substrates, mainly focusing on effects at elevated pump densities.

2. SAMPLE FABRICATION AND SETUP

The MLs have been mechanically exfoliated and isolated onto SiO_2/Si, hBN/Si_3N_4, and Sapphire (Al_2O_3). Here, hBN thickness is on the order of 10 nm and can be considered as the dominant substrate, while the refractive index of hBN and its substrate Si_3N_4 does not differ much (see [15]). For additional comparison, a sample with a chemical-vapour-deposition-grown (CVD) ML on Sapphire is included. The MLs (see Fig. 1) have been verified by the PL energy of the relevant mode both at room temperature (RT) and 10K (cf. Fig. 2), Raman signal (cf. Fig. 4) as well as optical contrast. The samples have been investigated

[1]The article is published in the original.
[2]These authors contributed equally.

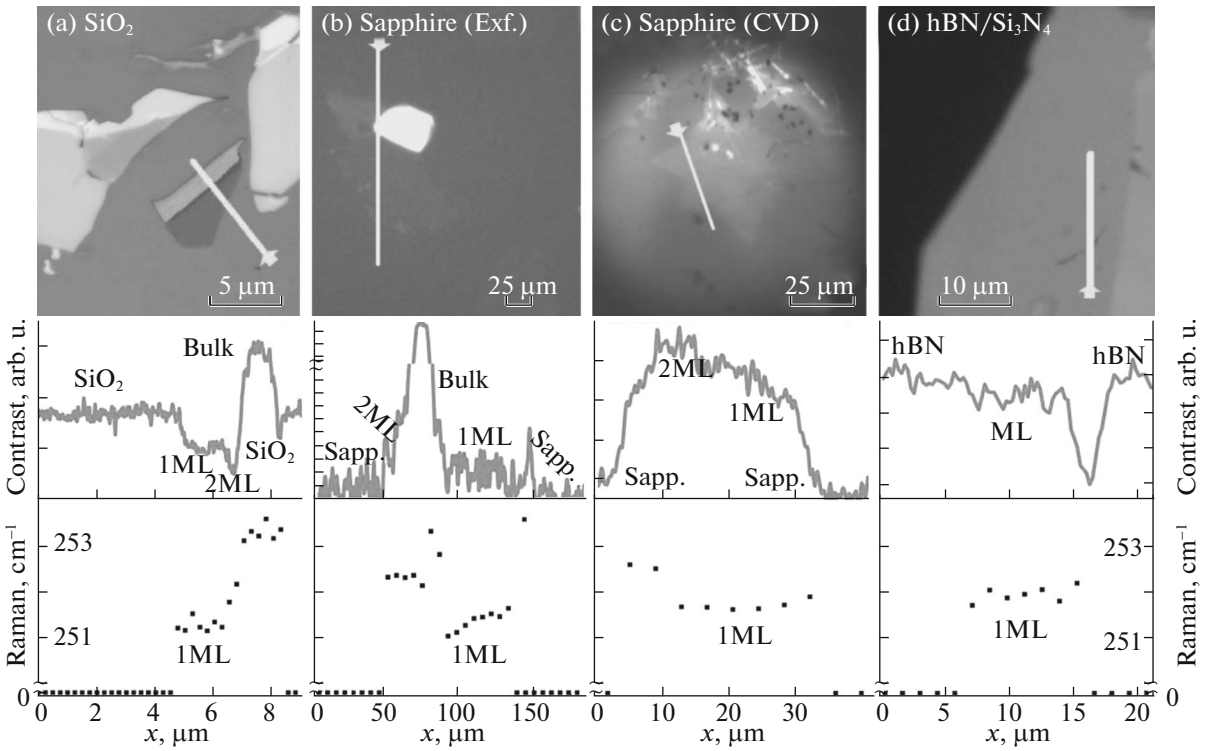

Fig. 1. (top) Microscope images of the samples with ML TMD coverage. (mid) Optical contrast charts representing cross sections along the line depicted in the micrographs above indicate the positions of ML material. (bottom) In addition to photoluminescence signatures, the peak positions of the corresponding Raman E_g^1 mode along the same line reveal the ML parts covering the substrate surface.

using a conventional μ-PL setup. A pulsed Ti:Sapphire laser with 100 fs temporal width has been used to excite the sample with the second harmonic (λ_{pump} = 445) nm. The emission was analysed in time-integrated or time-resolved mode using a spectrometer and a streak camera, respectively. For each of the samples, power-dependent spectra both at RT and at 10K and transients at RT have been measured.

3. RESULTS AND DISCUSSION

3.1. Spectra

The measured PL spectra for the power series are shown in Fig. 2. One can clearly observe the uprising of new excitonic features at 10K that have a different power dependence than the species obtained at RT. To further analyse the power dependence and their nature, the peaks have been fitted to the sum of two (RT) respectively four (10K) Gaussian peaks (see Fig. 2). The corresponding integrated intensities for these modes have been fitted to a power law (similar to [15, 23]) according to (Eq. (1)):

$$I_{PL} \propto P_{\text{pump}}^{\alpha}. \quad (1)$$

Here, P_{pump} refers to the excitation density and α is the linearity factor. The peaks at RT can be identified as localized trion and exciton in good agreement with the literature [24, 25] due to their energetic position and linearity factor being sublinear (see Fig. 3). Here, the excitation density dependent PL intensity is plotted over a span of nearly 3 orders of magnitude in pump fluence. From these charts, two linearity factors are extracted from two different excitation-density ranges for the set of ML-substrate samples (see analysis below). Interestingly, the CVD-grown sample exhibits the most free-exciton-like lower-fluence linearity factor in this measurement series. However, at 10K the observed spectra differ strongly. While on the one hand for the ML on SiO_2, for the CVD grown ML on Sapphire or the ML on hBN, the trion, exciton, biexciton [10] and trap state emission could be identified, on the other hand the exfoliated ML on Sapphire only unambiguously exhibits the exciton and some trap states at 10K. The identification is based on the α values obtained, the PL spectra and—determined in a separate measurement—the degree of circular polarization for the corresponding modes (data not shown here, see [15]).

3.2. Raman

To investigate possible strain for our set of ML-substrate samples, the Raman signature of WSe_2 around

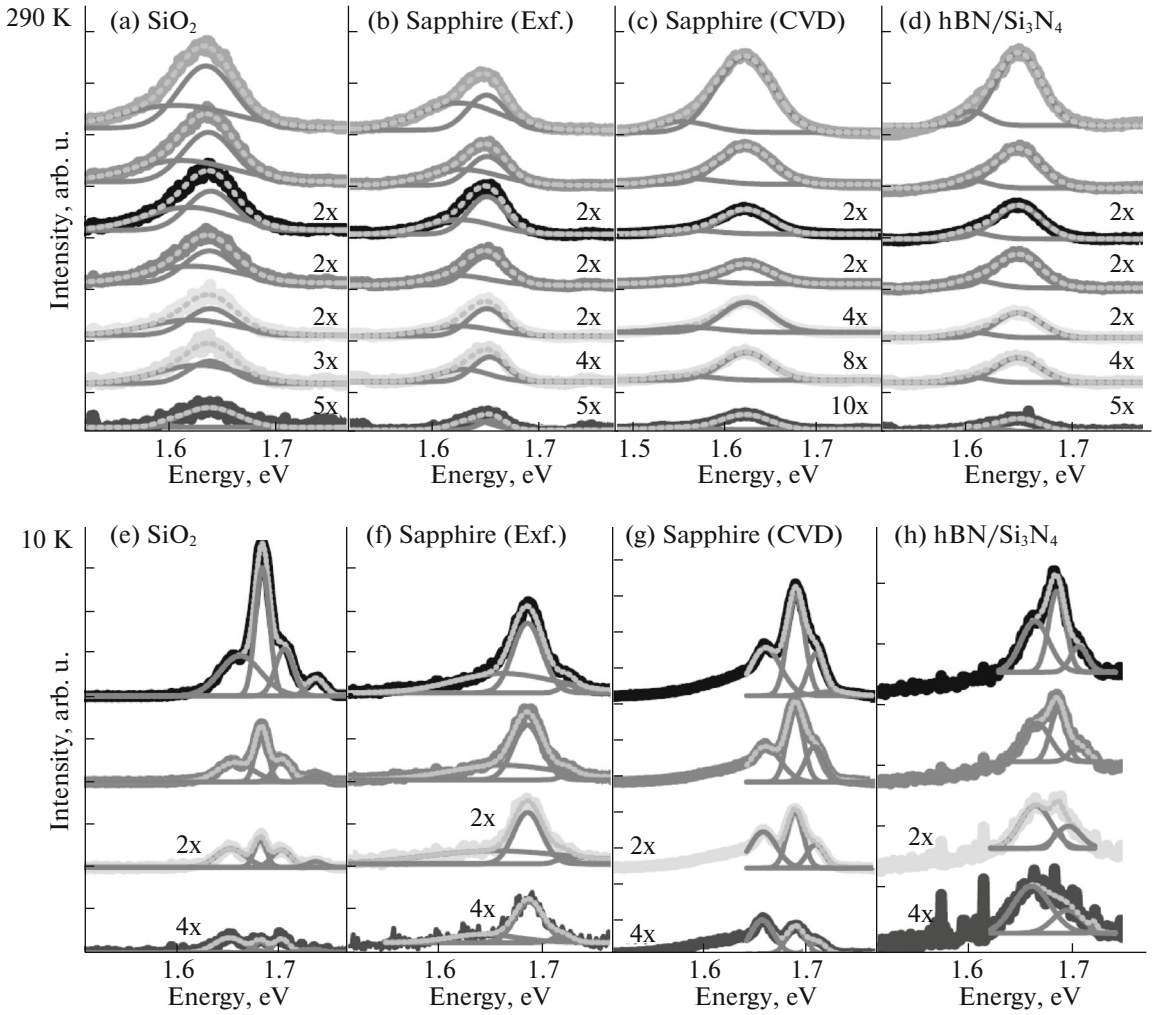

Fig. 2. (a–d) PL spectra of ML WSe_2 at room temperature. The shown excitation densities from the bottom to the top correspond to 300, 1000, 2150, 2900, 3400, 10000, 34000 W/cm^2. (e–h) Corresponding spectra recorded at 10K. The shown excitation densities from the bottom to the top correspond to 300, 1000, 2900, 3400 W/cm^2. For convenient comparison, the false-color-coded spectra at RT and 10 K are displayed in related colours. The Gaussian multi-peak fits (dotted light grey curve) that have been used for further analysis of the spectra are shown atop each of the curves (grey solid lines underneath it represent respective fits to the individual species).

250 to 260 cm^{-1} has been investigated (cf. Fig. 4). One can clearly see that the difference of the corresponding Raman-active modes A_g^1 and E_{2g}^1 are different for the samples. According to theoretical calculations of Sahin et al. [26] and Amin et al. [27], these modes increasingly split up by induced strain. The splitting is on average 16 cm^{-1} [26], starting from 11 cm^{-1} for zero strain. The corresponding positions are marked as grey dashed lines in Fig. 4. It is worth noting that the theoretical E_{2g}^1 mode position does not match experimental results and seems to have an offset of about 2 cm^{-1}. Nevertheless, the experimentally observed shift of the A_g^1 mode corresponds to a strain level of up to 1%. The different strain level for the exfoliated sample and the CVD-grown sample can have several reasons: either unintended introduction of strain in the exfoliation process, strain due to surface roughness of Sapphire, or the high temperatures at which the CVD growth takes place.

3.3. Power Dependence

The extracted peak intensities for the RT photoluminescence as a function of the pump density are shown in Fig. 3. One can clearly see that the pump-dependent data points exhibit a slightly sublinear power law up to a carrier density of approximately 5×10^{11} cm^{-2}. At even higher carrier densities, the emission indicates saturation behavior. Interestingly, the strength of saturation seems to depend strongly on the

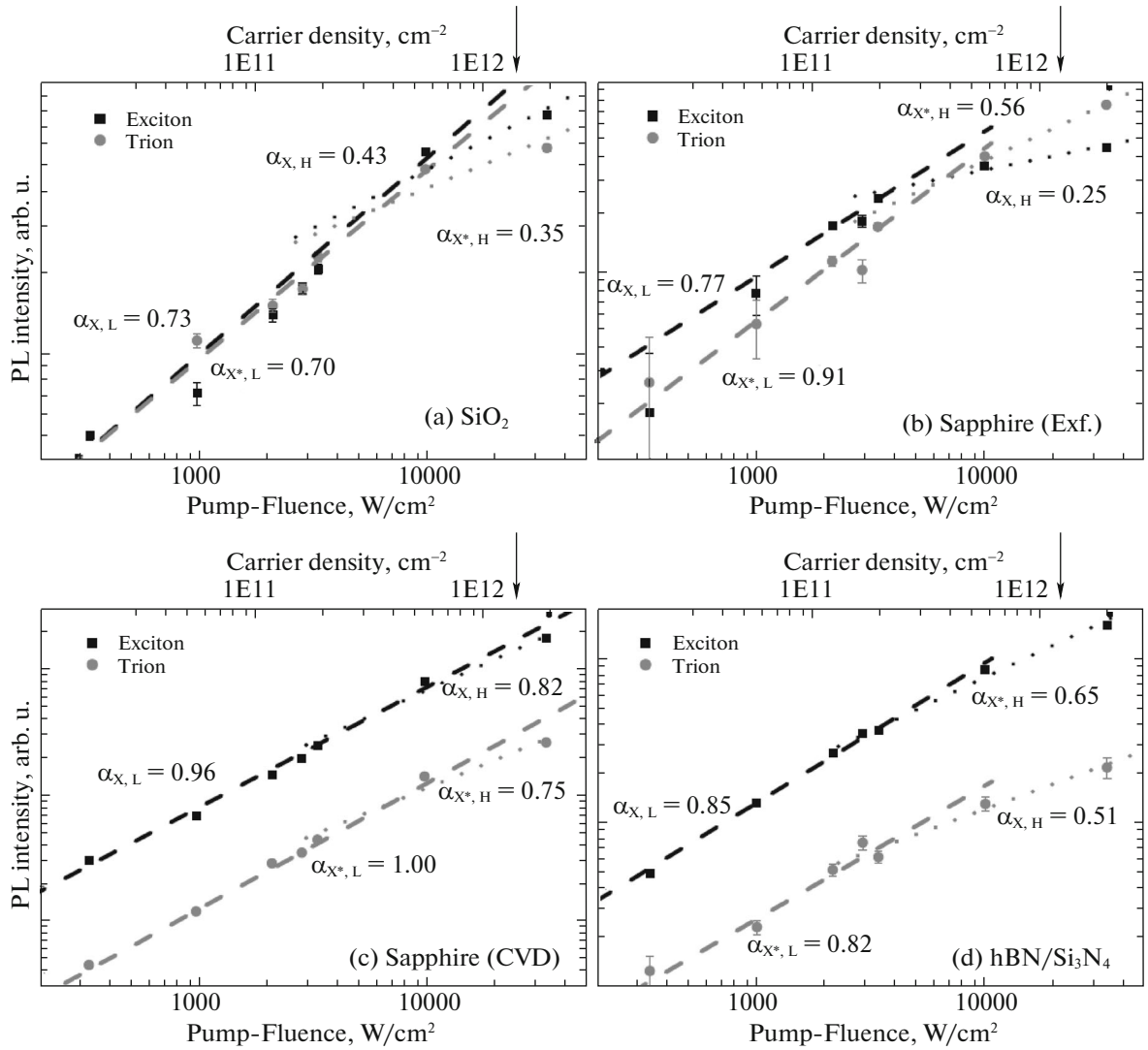

Fig. 3. PL intensity as a function of excitation density for different substrates at 290 K. The power dependence has been plotted on a double-logarithmic scale. The series have been fitted to a power law (dotted lines) to get a deeper insight into the recombination mechanism. The two data series for each sample correspond to the PL features that have been assigned to the exciton (black) and the trion (red). At elevated excitation densities there is a second power law fitted to the data revealing a lower slope indicating a Mott transition, with slopes representing an upper limit of α at these densities. The calculated Mott densities according to Eq. (3) are marked by a red arrow.

used substrate and fabrication method. To verify whether the slow-down can be associated with the onset of the Mott-transition [28], the Debye-Hückel screening length l_{DH} and the associated carrier density n_M were calculated using equations Eqs. (2) and (3).

$$l_{DH} = \left(\frac{\epsilon_0 \epsilon_{eff} k_B T}{8\pi e^2 n_p} \right)^{1/2}, \quad (2)$$

$$n_M = (1.19)^2 \frac{\epsilon_0 \epsilon_{eff} k_B T}{e^2 a_B}. \quad (3)$$

The effective permittivity ε_{eff} was calculated by the effective-medium approximation [29] using the volume fractions of the relevant materials within the Bohr radius a_B ($k_B T$ is the thermal energy, e the electron charge, and ε_0 the dielectric constant). The static permittivity ($\varepsilon_{eff}(\omega = 0)$) was used and the exciton Bohr radius follows the values obtained by Stier et al. [22]. The calculated values are summarized in Table 1. The hereby obtained Mott densities are marked by red arrows in Fig. 3. Comparing the calculated values with the measured data reveals that the change of slope in the input-output power plot could be explained by the onset of a Mott transition. Theoretically the smaller linearity factor has been predicted by Steinhoff [30] and was explained due to many-particle renormalization. The Σ valley lowers significantly more than the K

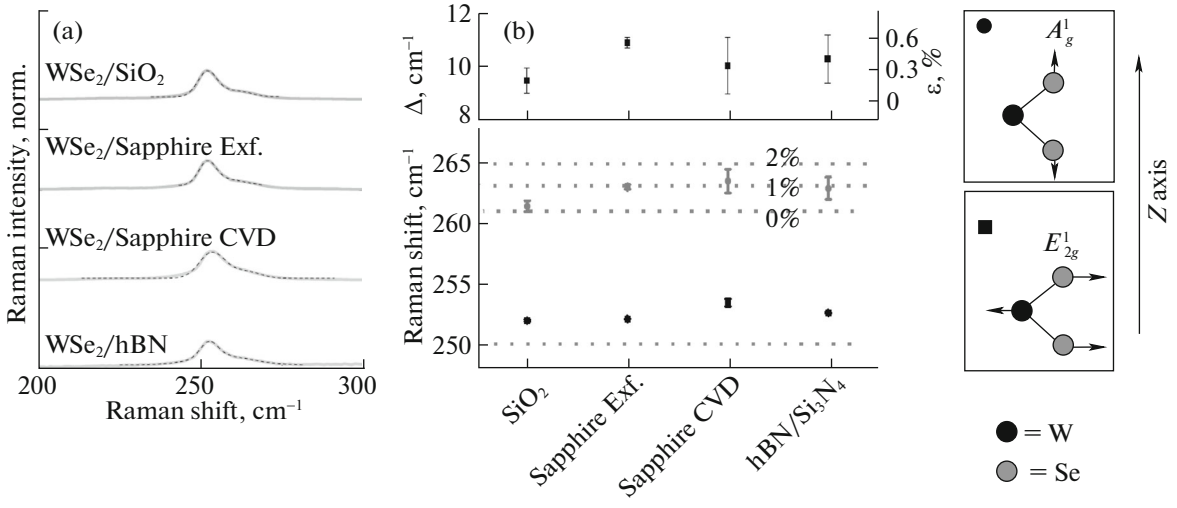

Fig. 4. (a) Raman spectra obtained for the four WSe_2-substrate combinations. (b) (lower graph) Peak position of the A_g^1 and E_{2g}^1 modes extracted by fitting the spectra with two Gaussians. The grey dashed lines indicate the calculated position of the A_g^1 mode with applied strain after [26]. The calculated E_{2g}^1 mode is located at 250 cm^{-1}. The strain values indicated in the chart correspond to these literature values for both modes. (upper graph) Total mode splitting shown with respect to the left scale and corresponding strain level ε in percent on the right scale for the measured modes. On the right hand side, the two respective Raman modes are sketched for illustration.

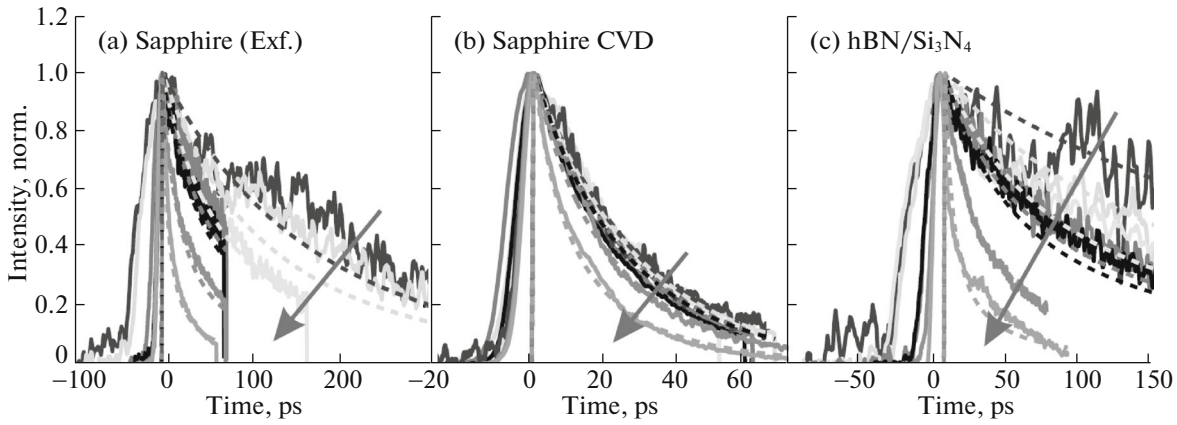

Fig. 5. Observation and modelling of exciton–exciton annihilation. Representative transient-PL traces measured at 290 K for three samples (a–c) from our set of ML-substrate combinations are shown here as solid curves. The transients have been fitted with a bimolecular function (according to Eqs. (4) and (5), dashed curves). The shortening of the decay times with increasing excitation density (marked by red arrows) can be well explained by a diffusion-mediated annihilation process, as the fit function can reproduce the measured trends correctly. The excitation densities shown are the same as in Fig. 2.

valley, which leads to a carrier drain and the band gap becomes indirect. The many-body calculation predicts a linear slope up to a carrier density of 3×10^{12} cm^{-2} [30]. To extract the relevant excitation density (pump fluence) for that onset, a measurement with smaller pump fluence steps is necessary.

3.4. Decay Dynamics

Next, spectrally-integrated transients for three of our samples are shown in Fig. 5. (The SiO_2 sample degraded before the TRPL measurements.) A pronounced shortening is observed as a function of increased pump power. To test whether this arises from exciton–exciton annihilation as proposed and discussed by Mouri et al. [31], the transient-PL series have been modelled with a rate equation (Eqs. (4) and (5)) after [32, 33]:

$$\frac{dN}{dt} = G(t) - \frac{N}{\tau} - \xi_{2D} N^2, \quad (4)$$

Table 1. Obtained values for the electric permittivity (after the effective-medium approximation), the calculated Mott density and the corresponding screening length (according to Eqs. (2) and (3))

Substrate	ε_{eff}	n_M (10^{12} cm^{-2})	l_{DH}(Å)
SiO_2	9.04	1.473	5.270
Sapphire (exf.)	8.63	1.250	5.825
Sapphire (CVD)	8.63	1.250	5.825
hBN	8.61	1.123	6.305

Table 2. Fit parameters for the diffusion-mediated exciton–exciton annihilation model applied to the data shown in Fig. 5

Substrate	τ (ps)	D (nm^2/ps)	a_B (nm)
SiO_2	–	–	1.20
Sapphire (exf.)	188	50	1.35
Sapphire (CVD)	28.5	26.8	1.35
hBN	362	35	1.50

$$\xi_{2D} = \frac{4\pi D}{\log\left(\frac{1}{2}\sqrt{\frac{1}{Dt}}R_e\right)}. \quad (5)$$

The simulation (see dashed lines in Fig. 5) matches with the observed transients and the extracted annihilation rates for these samples are similar to those in [31]. Nevertheless, the observed rates vary in a comparison of the used substrates. The CVD-grown sample shows a different pump-fluence-dependent behavior compared to the exfoliated samples on Sapphire and hBN substrates. The fit parameters are shown in Table 2. Here, the exciton Bohr radius for SiO_2 and hBN was taken from [22] and was not used as a fit parameter. The Bohr radius for Sapphire has been interpolated. The values are the same as used in Eq. (3). The determined diffusion constants D are of the same order but slightly bigger than previously reported values [34, 35].

A more systematic comparison of these parameters in such a bimolecular fit as a function of the environment of WSe_2 monolayers can be found in [23]. In general, it can be assumed that for a decreasing Bohr radius, the diffusion constant increases as is found here. Yet, the difference between exfoliated and CVD-grown ML on Sapphire shall be explained by different strain levels, monolayer quality and surface-related effects due to the different sample production methods. Clearly, the difference between the low-pump-fluence decay times can arise from those circumstances, which can directly affect the diffusion constant. The faster decaying PL in the CVD-grown ML in comparison with the exfoliated counterpart correlates well/directly with the significant reduction of D. Seemingly, CVD-grown MLs are less prone to such excitation-density dependent decay mechanism, as the general decay is considerably faster and the diffusion constant smaller. Ultimately, the role of hBN used as buffer and encapsulant is of great importance for the emission and dynamics of ML systems, as is discussed in detail in [23].

4. CONCLUSION

In summary, two-dimensional (2D) WSe_2 in the monolayer regime on a set of substrates commonly used in applications, both opaque (i.e. oxides/nitrides on Si wafer) and transparent (Sapphire, hBN), has been systematically investigated by means of μ-Raman, μ-PL, and μ-TRPL. The obtained results show similarities in the decay dynamics like the observation of exciton–exciton annihilation at RT and indicate strong comparability of the ML spectra in terms of mode energies at both elevated and cryogenic temperatures. Nevertheless, subtle changes become evident such as the occurrence of different annihilation rates, time and diffusion constants and the appearance of different 2D-excitonic modes at low temperature. Here, our substrate-dependent investigation for different pump-fluences further allowed us to shed light on variations in the exciton Bohr radius and the Mott density at RT. Indeed, this study invites to a more sophisticated analysis of the substrate–monolayer interactions which is of great importance for the tailoring of 2D-material-based opto-electronic structures.

ACKNOWLEDGMENTS

The authors acknowledge financial support by the Philipps-Universität Marburg, the German Research Foundation (DFG: SFB1083) and the German Academic Exchange Service (DAAD). Work at Columbia was funded by the NSF MRSEC under DMR-1420634.

REFERENCES

1. K. F. Mak, C. Lee, J. Hone, J. Shan, and T. F. Heinz, Phys. Rev. Lett. **105**, 136805 (2010). doi 10.1103/PhysRevLett.105.136805
2. G. Wang, A. Chernikov, M. M. Glazov, T. F. Heinz, X. Marie, T. Amand, and B. Urbaszek, arXiv:1707.05863 (2017).
3. L. Britnell, R. M. Ribeiro, A. Eckmann, R. Jalil, B. D. Belle, A. Mishchenko, Y. J. Kim, R. V. Gorbachev, T. Georgiou, S. V. Morozov, A. N. Grigorenko, A. K. Geim, C. Casiraghi, A. H. C. Neto, and K. S. Novoselov, Science (Washington, DC, U. S.) **340** (6138), 1311 (2013). doi 10.1126/science.1235547
4. B. Radisavljevic, A. Radenovic, J. Brivio, V. Giacometti, and A. Kis, Nat. Nanotechnol. **6**, 147 (2011). doi 10.1038/nnano.2010.279
5. S. Das, M. Dubey, and A. Roelofs, Appl. Phys. Lett. **105**, 083511 (2014). doi 10.1063/1.4894426

6. F. Withers, O. del Pozo-Zamudio, S. Schwarz, S. Dufferwiel, P. M. Walker, T. Godde, A. P. Rooney, A. Gholinia, C. R. Woods, P. Blake, S. J. Haigh, K. Watanabe, T. Taniguchi, I. L. Aleiner, A. K. Geim, V. I. Fal'ko, A. I. Tartakovskii, and K. S. Novoselov, Nano Lett. **15**, 8223 (2015). doi 10.1021/acs.nanolett.5b03740
7. H. Li, J. Wu, Z. Yin, and H. Zhang, Accounts Chem. Res. **47**, 1067 (2014). doi 10.1021/ar4002312
8. E. Cappelluti, R. Roldán, J. A. Silva-Guillén, P. Ordejón, and F. Guinea, Phys. Rev. B **88**, 075409 (2013). doi 10.1103/PhysRevB.88.075409
9. A. Chernikov, T. C. Berkelbach, H. M. Hill, A. Rigosi, Y. Li, O. B. Aslan, D. R. Reichman, M. S. Hybertsen, and T. F. Heinz, Phys. Rev. Lett. **113**, 076802 (2014). doi 10.1103/PhysRevLett.113.076802
10. Y. You, X. X. Zhang, T. C. Berkelbach, M. S. Hybertsen, D. R. Reichman, and T. F. Heinz, Nat. Phys. **11**, 477 (2015). doi 10.1038/nphys3324
11. M. Danovich, V. Zólyomi, and V. I. Fal'ko, Sci. Rep. **7**, 45998 (2017). doi 10.1038/srep45998
12. K. Hao, J. F. Specht, P. Nagler, L. Xu, K. Tran, A. Singh, C. K. Dass, C. Schüller, T. Korn, M. Richter, A. Knorr, X. Li, and G. Moody, Nat. Commun. **8**, 15552 (2017). doi 10.1038/ncomms15552
13. Y. Yu, Y. Yu, C. Xu, A. Barrette, K. Gundogdu, and L. Cao, Phys. Rev. B **93**, 201111 (2016). doi 10.1103/PhysRevB.93.201111
14. L. Yuan and L. Huang, Nanoscale **7**, 7402 (2015). doi 10.1039/C5NR00383K
15. S. Lippert, L. M. Schneider, D. Renaud, K. N. Kang, O. Ajayi, J. Kuhnert, M. U. Halbich, O. M. Abdulmunem, X. Lin, K. Hassoon, S. Edalati-Boostan, Y. D. Kim, W. Heimbrodt, E. H. Yang, J. C. Hone, and A. Rahimi-Iman, 2D Mater. **4**, 025045 (2017). doi 10.1088/2053-1583/aa5b21
16. D. Sun, Y. Rao, G. A. Reider, G. Chen, Y. You, L. Brézin, A. R. Harutyunyan, and T. F. Heinz, Nano Lett. **14**, 5625 (2014). doi 10.1021/nl5021975
17. N. Kumar, Q. Cui, F. Ceballos, D. He, Y. Wang, and H. Zhao, Phys. Rev. B **89**, 125427 (2014). doi 10.1103/PhysRevB.89.125427
18. A. Chernikov, C. Ruppert, H. M. Hill, A. F. Rigosi, and T. F. Heinz, Nat. Photon. **9**, 466 (2015). doi 10.1038/nphoton.2015.104
19. A. F. Rigosi, H. M. Hill, Y. Li, A. Chernikov, and T. F. Heinz, Nano Lett. **15**, 5033 (2015). doi 10.1021/acs.nanolett.5b01055
20. Y. Lin, X. Ling, L. Yu, S. Huang, A. L. Hsu, Y. H. Lee, J. Kong, M. S. Dresselhaus, and T. Palacios, Nano Lett. **14**, 5569 (2014). doi 10.1021/nl501988y
21. Y. Yu, Y. Yu, C. Xu, Y. Q. Cai, L. Su, Y. W. Zhang, Y. W. Zhang, K. Gundogdu, and L. Cao, Adv. Funct. Mater. **26**, 4733 (2016). doi 10.1002/adfm.201600418
22. A. V. Stier, N. P. Wilson, G. Clark, X. Xu, and S. A. Crooker, Nano Lett. **16**, 7054 (2016). doi 10.1021/acs.nanolett.6b03276
23. L. M. Schneider, S. Lippert, J. Kuhnert, O. Ajayi, D. Renaud, S. Firoozabadi, Q. Ngo, R. Guo, Y. D. Kim, W. Heimbrodt, J. C. Hone, and A. Rahimi-Iman, Nano-Struct. Nano-Objects (2017). doi 10.1016/j.nanoso.2017.08.009
24. T. Godde, D. Schmidt, J. Schmutzler, M. Aßmann, J. Debus, F. Withers, E. M. Alexeev, O. del Pozo-Zamudio, O. V. Skrypka, K. S. Novoselov, M. Bayer, and A. I. Tartakovskii, Phys. Rev. B **94**, 165301 (2016). doi 10.1103/PhysRevB.94.165301
25. J. Huang, T. B. Hoang, and M. H. Mikkelsen, Sci. Rep. **6**, 22414 (2016). doi 10.1038/srep22414
26. H. Sahin, S. Tongay, S. Horzum, W. Fan, J. Zhou, J. Li, J. Wu, and F. M. Peeters, Phys. Rev. B **87**, 165409 (2013). doi 10.1103/PhysRevB.87.165409
27. B. Amin, T. P. Kaloni, and U. Schwingenschlögl, RSC Adv. **4**, 34561 (2014). doi 10.1039/C4RA06378C
28. C. Klingshirn, *Semiconductor Optics* (Springer, Berlin, Heidelberg, 2007). doi 10.1007/978-3-540-38347-5
29. von K. Rottkay, T. Richardson, M. Rubin, and J. Slack, in *Optical Materials Technology for Energy Efficiency and Solar Energy Conversion XV,* Proc. SPIE **3138**, 9 (1997).
30. A. Steinhoff, J. H. Kim, F. Jahnke, M. Rösner, D. S. Kim, C. Lee, G. H. Han, M. S. Jeong, T. O. Wehling, and C. Gies, Nano Lett. **15**, 6841 (2015). doi 10.1021/acs.nanolett.5b02719
31. S. Mouri, Y. Miyauchi, M. Toh, W. Zhao, G. Eda, and K. Matsuda, Phys. Rev. B **90**, 155449 (2014). doi 10.1103/PhysRevB.90.155449
32. C. Daniel, L. M. Herz, C. Silva, F. J. M. Hoeben, P. Jonkheijm, A. P. H. J. Schenning, and E. W. Meijer, Phys. Rev. B **68**, 235212 (2003). doi 10.1103/PhysRevB.68.235212
33. A. Suna, Phys. Rev. B **1**, 1716 (1970). doi 10.1103/PhysRevB.1.1716
34. K. D. Park, O. Khatib, V. Kravtsov, G. Clark, X. Xu, and M. B. Raschke, Nano Lett. **16**, 2621 (2016). doi 10.1021/acs.nanolett.6b00238
35. A. M. van der Zande, P. Y. Huang, D. A. Chenet, T. C. Berkelbach, Y. You, G. H. Lee, T. F. Heinz, D. R. Reichman, D. A. Muller, and J. C. Hone, Nat. Mater. **12**, 554 (2013). doi 10.1038/nmat3633